Au−Pd Nanoparticles Dispersed on Composite Titania/Graphene Oxide-Supports as a Highly Active Oxidation Catalyst

Jiacheng Wang,[†,‡] Simon A. Kondrat,[‡] Yingyu Wang,[‡] Gemma L. Brett,[‡] Cicely Giles,[‡] Jonathan K. Bartley,[‡] Li Lu,[§] Qian Liu,[†] Christopher J. Kiely,[§] and Graham J. Hutchings*[,‡]

[†]State Key Laboratory of High Performance Ceramics and Superfine Microstructure, Shanghai Institute of Ceramics, Chinese Academy of Sciences, Shanghai 200050, P. R. China
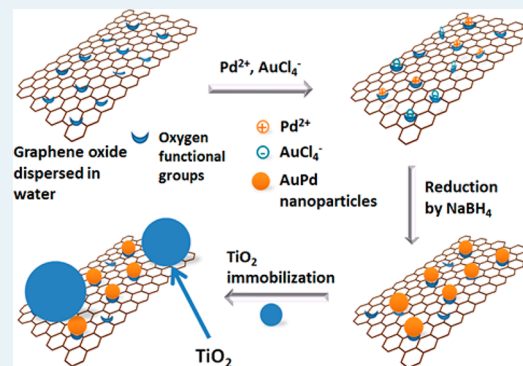
[‡]Cardiff Catalysis Institute, School of Chemistry, Cardiff University, Main Building, Park Place, Cardiff, CF10 3AT, U.K.

[§]Department of Materials Science and Engineering, Lehigh University, 5 East Packer Avenue, Bethlehem, Pennsylvania 18015-3195, United States

Ⓢ Supporting Information

ABSTRACT: The control over both the dispersion and the particle size distribution of supported precious metal nanoparticles used in heterogeneous catalysts is of paramount importance. Here, we demonstrate the successful formation of highly accessible and well dispersed gold−palladium nanoparticles, stabilized with two-dimensional graphene oxide, that itself is dispersed by intercalated titania particles to form ternary hybrid catalysts. In this application, graphene oxide acts as an effective substitute for the more conventional polymer ligands that are used to stabilize nanoparticles in a sol-immobilization procedure. The particle size distribution can be adjusted by varying the graphene oxide-to-metal mass ratio. The addition of titania efficiently hinders the stacking and agglomeration of the supported metal on graphene oxide sheets, facilitating diffusion of oxygen and reactants to the catalyst surface. This gold−palladium/graphene oxide/titania "ternary" catalyst has been tested for the selective oxidation of a range of alcohols. The resulting optimized catalyst exhibits a comparable activity to a sol-immobilized derived catalyst where the metal nanoparticles are stabilized by poly(vinyl alcohol) ligands, with the graphene oxide-stabilized hybrid catalyst having enhanced stability. We consider that the novel strategy of supporting metal nanoparticles described here can also be adopted to synthesize a wide range of high activity, stable heterogeneous catalysts for other reactions.

KEYWORDS: *graphene oxide/titania catalyst composites, graphene oxide nanoparticle stabilizer, gold−palladium nanoalloy, bimetallic nanoparticles, selective alcohol oxidation*

Heterogeneous catalysis is a key process in the manufacture of a wide range of chemicals and is at the heart of green chemical processes. Au nanoparticles (NPs) have been shown to be effective for the oxidation of alkenes[1−4] and alcohols,[5,6] the oxidation of CO at low temperatures,[7] and for the direct synthesis of hydrogen peroxide (H_2O_2).[8,9] Furthermore, it has been demonstrated that alloying Au with Pd results in a significant enhancement in activity for alcohol oxidation[10] and also markedly improves the yield of H_2O_2 in the direct synthesis reaction.[10,11] Usually, these metal NPs are immobilized on inorganic supports such as refractory metal oxides, (e.g., TiO_2), and a variety of carbon supports (e.g., activated carbon, graphite, carbon nanotubes (CNTs)), to reduce the cost of the catalysts and improve the catalytic activity and stability.

Since the seminal work of Geim and co-workers on the preparation of single layer graphene,[12] immense scientific excitement has ensued, with graphene and modified graphene structures being shown to have notable and potentially exploitable electronic,[12] optical,[13] and other physical properties.[14,15] Graphene oxide (GO) has primarily been used as a precursor in the production of graphene and other function-alized graphene structures.[16−18] However, GO is now beginning to gain interest in its own right, due to its own particular chemical and electronic characteristics. Tuning the ratio of sp[2] and sp[3] hybridized carbon atoms in GO provides the possibility of tailoring optical and electronic properties,[19] while the array of possible oxygen containing functional groups that can associate with GO has been found to catalyze certain oxidation and hydration reactions.[20,21] These functional groups also allow for attachment and decoration of GO with various metal NPs for a range of electronic, charge storage, sensor and catalysis applications.[22] Specifically Au or Pd NPs supported on GO have been explored as catalysts for Suzuki−Miyaura

coupling reactions[23−25] and Fe based Fischer−Tropsch catalysts,[26] while Pt and Pt−Pd NPs supported on GO have been studied for methanol electro-oxidation.[27,28] Further to this, magnetic iron oxide (up 30 wt %) has been incorporated into a Pd/graphene Suzuki−Miyaura coupling catalyst to enhance recyclability after reaction by utilizing its magnetic properties to separate the catalyst from the reaction products.[29]

GO has not only hydrophilic (i.e., hydroxyl and carboxyl) groups, allowing it to be dispersed in water,[30] but also comprises hydrophobic nanographene domains on the basal plane (see Supporting Information, Figure S1). Thus, GO is a flexible amphiphile with surfactant-like properties.[31] Sol-immobilization using metal sols prepared with organic surfactants such as poly(vinyl alcohol) (PVA) or polyvinylpyr-rolidone (PVP) is a highly successful technique for making supported Au and Au−Pd catalysts that gives a high degree of control over particle size distribution (PSD) and morphol-ogy.[32−34] However, the presence of organic surfactants ligands on the supported sol-derived metal NPs frequently, but not universally, decreases the activity of the catalysts because of the blocking of active sites. Consequently, treatments for removing the organic ligands are often necessary, including thermal and oxidative approaches, which not only result in significant changes in the size and shape of NPs but also limit the choice of supports.[35,36] Recently, we reported that ∼20% of the PVA stabilizing ligand in supported sol-derived metal NPs could be removed by a simple treatment involving refluxing with hot water,[37] which improves the surface exposure of the metal NPs and enhances their catalytic activity for a range of reactions. More recently, by adopting a convenient excess anion modification and postreduction step, supported bimetallic Au−Pd NPs with a narrow PSD were also successfully prepared without the complication of having organic surfactant molecules adsorbed on the active metal NP surface.[38]

In this paper we show that Au−Pd alloy NPs can be stabilized using exfoliated flexible GO sheets in place of organic surfactants, such as PVA and PVP (see Supporting Information, Figure S2). These GO sheets decorated with metal NPs were then intimately dispersed with TiO$_2$ particles and utilized as a highly efficient, stable, recyclable catalyst for solvent-free oxidation of alcohols with molecular oxygen. These AuPd/GO/TiO$_2$ materials often showed superior catalytic properties to the more conventional PVA-stabilized sol immobilized materials. The dispersion of AuPd/GO with TiO$_2$ was investigated in an attempt to inhibit efficient stacking of the GO layers, due to $\pi-\pi$ bonding interactions, thus promoting the diffusion of alcohols and oxygen molecules between adjacent GO sheets. The combination of TiO$_2$ intercalation between GO sheets and uncoated Au−Pd NPs improves the surface exposure of the catalytic active sites and significantly enhances the catalytic activity.
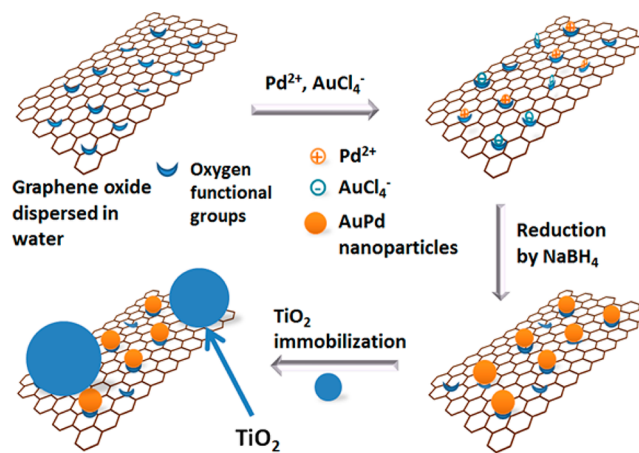
■ RESULTS AND DISCUSSION

Catalyst Preparation and Structural Characterization. The purpose of this study was the preparation and testing of Au and Au−Pd catalysts immobilized onto GO without the use of surfactant molecules such as PVA. For the purposes of understanding the motivation and progression of the work, we will highlight certain features and parameters of the catalyst preparation method, but for an in-depth description of catalyst preparation protocols, please refer to the Methods section. An illustration of the preparation protocol for generating GO stabilized Au−Pd NPs on TiO$_2$ (AuPd−GO/TiO$_2$) is shown in

Scheme 1. Water dispersed GO prepared from graphitic oxide (GTO), synthesized according to the method of Hummers and

Scheme 1. Illustration of the Method Used for Preparing GO Stabilized Au−Pd NPs on TiO$_2$ (AuPd−GO/TiO$_2$) Using a "Ligand-free" Sol-Immobilization-Type Approach

Offeman,[39] was introduced into a HAuCl$_4$ and PdCl$_2$ solution. Subsequently, the metals were reduced using NaBH$_4$, *without* the addition of a surfactant, to form Au−Pd NPs stabilized solely by GO (denoted hereafter as AuPd−GO). This material was then characterized and tested for a range of catalytic reactions, to provide an understanding of the binary metal−GO system. To form the AuPd−GO/TiO$_2$ ternary material, TiO$_2$ was added to the AuPd−GO suspension. For comparison, PVA sol-immobilized Au−Pd NPs supported on TiO$_2$ (denoted AuPd−PVA/TiO$_2$) were also prepared using a similar method.

Transmission electron microscopy (TEM) images (Figure 1a) demonstrate that GO was successfully exfoliated in water with the corresponding selected area diffraction (SAD) pattern (inset, Figure 1a) confirming the identity of GO (also see Supporting Information, Table S1). The individual GO sheets had lateral dimensions ranging between 50 nm and 1 μm. TEM analysis of the resulting AuPd−GO assemblies retrieved from the suspension confirmed the successful loading of Au−Pd NPs onto the GO sheets. A representative high-magnification TEM image of a 1:4 AuPd:GO assembly, displayed in Figure 1b, reveals that the GO-stabilized Au−Pd NPs range between 1 and 7 nm in size, and the corresponding particle size distribution (Figure 1c) indicates that the mean particle size is 2.8 nm. Unlike a PVA or PVP stabilized NPs where the polymer provides a 3-dimensional encapsulation, the AuPd:GO would act as a 2-dimensional stabilizer (as visualized in Scheme 1).

TiO$_2$ would then be added to the suspended AuPd−GO material to form the final ternary 1 wt % AuPd−GO/TiO$_2$ catalyst. The contribution of metal (AuPd) within all catalysts was fixed at 1 wt %, with the GO:TiO$_2$ ratio being altered to give GO compositions between 1 and 9 wt %. Therefore, the metal:GO ratio would significantly alter between 1 wt % AuPd−1 wt % GO/TiO$_2$ and 1 wt % AuPd/9 wt % GO/TiO$_2$. The corresponding metal:GO weight ratios would vary from 1:1 to 1:9 between the 1 wt % AuPd−1 wt % GO/TiO$_2$ and 1 wt % AuPd−9 wt % GO/TiO$_2$ materials. For example, the 1:4 ratio of metal:GO in the sample shown in Figure 1b, would be required to make a final 1 wt % AuPd−4 wt % GO/95 wt % TiO$_2$ hybrid catalyst. The metal:GO weight ratios for all the
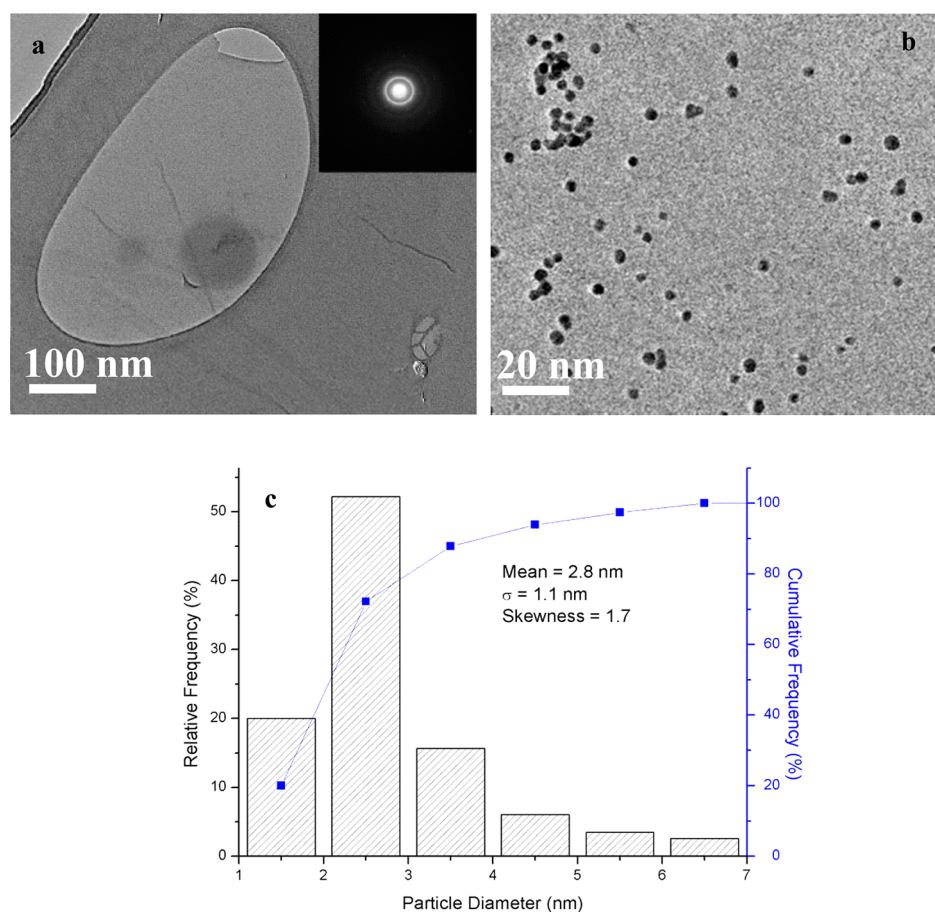
Figure 1. (a) Representative TEM image of the exfoliated GO sheet with the corresponding SAD pattern inset; (b) Au−Pd alloy NPs stabilized by the GO sheet (AuPd:GO of 1:4) along with (c) a particle size distribution (PSD) for the Au−Pd NPs (100 particles counted) .
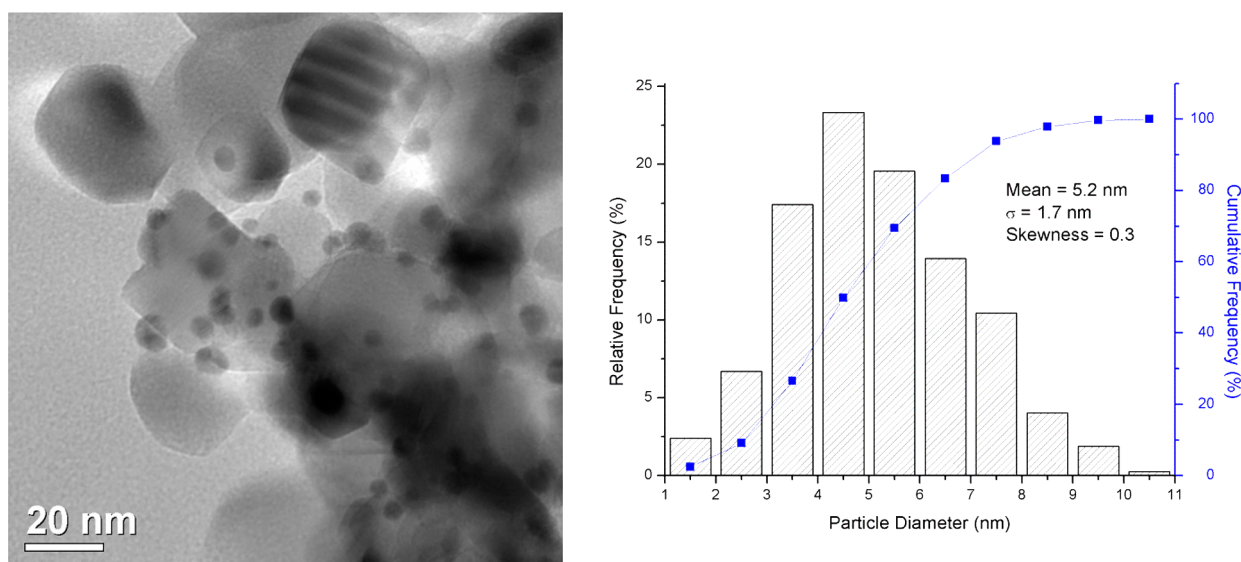

Figure 2. Representative BF-TEM micrograph and corresponding PSD of the 1 wt % AuPd−PVA/TiO$_2$ sample (100 particles counted).

binary AuPd/GO compositions investigated in this work are summarized in Table S2. The ability to disperse such high metal weight loadings, while still retaining such a small particle size, demonstrates the efficacy of GO in stabilizing Au−Pd NPs, due to its high number of potential anchoring sites.

In common with the sol-immobilization route using PVA stabilized AuPd particles, the AuPd−GO entities were also immobilized by supporting them on TiO$_2$. The resultant AuPd−PVA/TiO$_2$ and AuPd−GO/TiO$_2$ counterpart materials were further characterized and compared. Elemental analysis, determined by microwave plasma-atomic emission spectroscopy, revealed that all the AuPd−GO/TiO$_2$ composite materials had close to their target 1:1 molar Au:Pd ratios with weight loadings of ca. 0.8 wt % (i.e., slightly lower than the expected
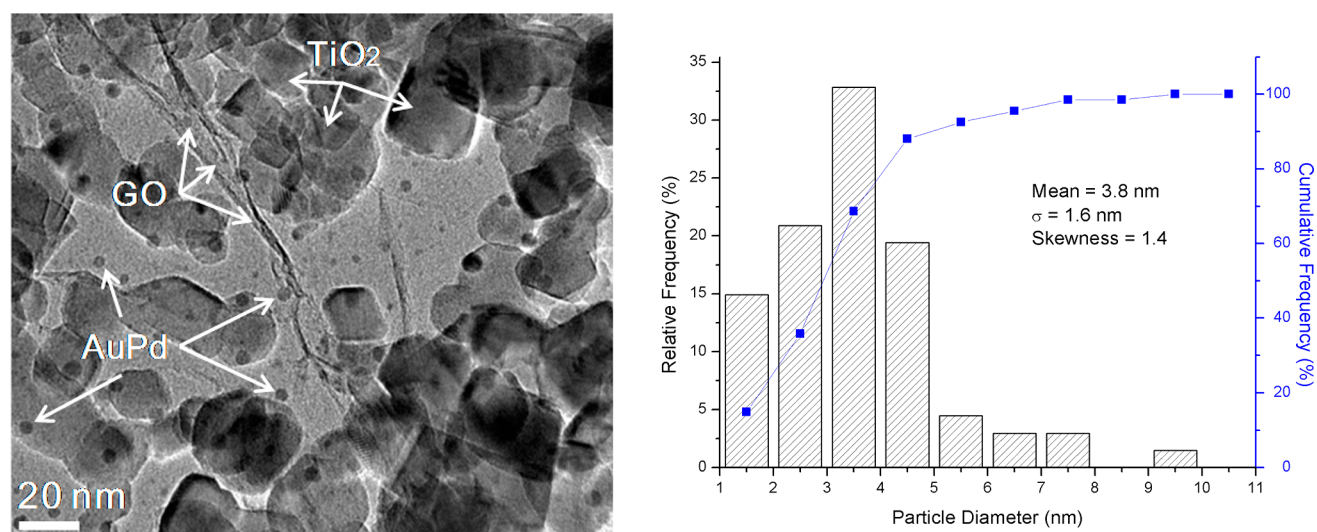
Figure 3. Representative BF-TEM micrograph of the AuPd−9% GO/TiO$_2$ sample. (inset) Corresponding Au−Pd particle size distribution (PSD) (100 particles counted).
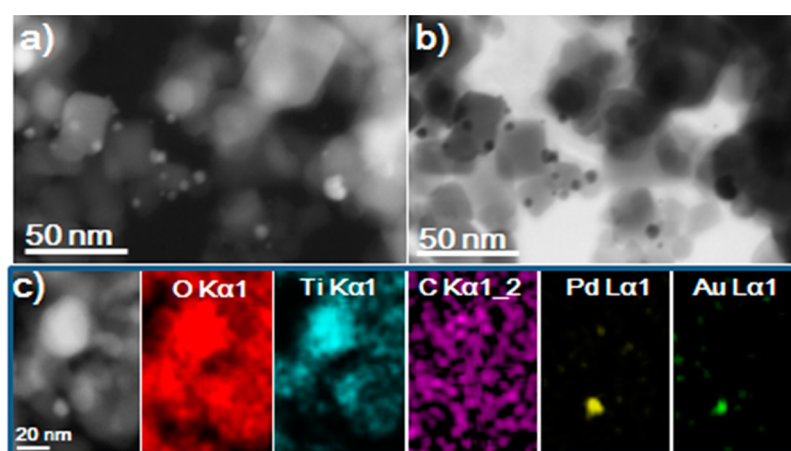

Figure 4. Simultaneously acquired (a) HAADF-STEM and (b) BF-STEM micrographs of AuPd−4% GO/TiO$_2$. (c) Complementary O K$_{\alpha1}$, Ti K$_{\alpha1}$, C K$_{\alpha1}$, Pd L$_{\alpha1}$, and Au L$_{\alpha1}$ XEDS elemental maps obtained from the region shown in the HAADF-STEM image on the far left.

nominal 1 wt % loading) (see Table S3). Both the Au and Pd components present in the AuPd−PVA/TiO$_2$ and AuPd−GO/TiO$_2$ catalysts were found to be in a metallic state from XPS analysis (Figure S3). Bright field (BF) TEM analysis of the conventional 1 wt %AuPd−PVA/TiO$_2$ sample showed that the alloyed metal nanoparticles have a mean size of 5.2 nm and are in close contact with the TiO$_2$ support particles (see Figure 2) as was noted in previously published work.[40] Comparable BF-TEM analysis of the AuPd−GO/TiO$_2$ materials showed that they were a highly mixed composite structure comprising TiO$_2$ particles, GO sheets, and small AuPd NPs (Figure 3). As with the binary AuPd−GO material, Au−Pd NPs were predominantly associated with the GO sheets, although some fraction of these NPs may well have direct physical contact with the TiO$_2$. The GO sheets, whose identity was confirmed by electron diffraction analysis (Figure S4), are dispersed among the TiO$_2$ particles, which serve to hinder GO aggregation into lower surface area structures. Representative high angle annular dark field (HAADF) and BF-STEM images of the AuPd−4% GO/TiO$_2$ sample are shown in Figures 4a and 4b, respectively. X-ray energy dispersive (XEDS) mapping (Figure 4c) confirms the that the metal NPs in the materials are indeed AuPd alloys

and also suggests that the GO sheets are intimately mixed with the TiO$_2$ particles in the composite support.

Powder X-ray diffraction shows that GTO exfoliation in the presence of TiO$_2$ inhibited GO sheet agglomeration, with the reflection of the basal [001] plane indicative of ordered graphitic oxide (GTO), being no longer observable in a 6 wt % GO/TiO$_2$ composite support material (Figure 5). This loss of order has previously been attributed to the reduction of GO.[25] This is not possible for the 6 wt % GO/TiO$_2$ composite as there was no addition of reducing agent; the loss of the [001] plane can only be due to TiO$_2$ preventing the long-range stacking of GO. We hypothesized that these mixed GO/TiO$_2$ support structures, with their inherent frustrated GO stacking, when used as a support for Au−Pd NP's could potentially increase the accessibility of reactants to the Au−Pd NPs. This intriguing possibility is explored and discussed further in subsequent sections.

The AuPd particle size distributions (PSDs) for all the AuPd−GO/TiO$_2$ catalysts studied, as derived from analysis of BF-TEM images (see Supporting Information, Figure S5), are presented in Figure 6 and summarized in Table 1. With the conventional PVA surfactant, the median Au−Pd particle size
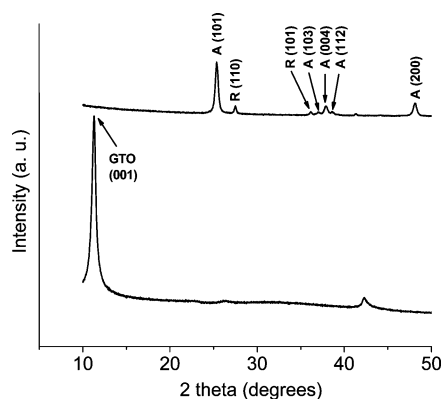
Figure 5. XRD patterns of (*below*) graphite oxide (GTO) and (*above*) 6 wt % GO/TiO$_2$. The XRD pattern of GTO shows a reflection characteristic of the GTO (001) plane. By exfoliating the GTO in water by ultrasonication in the presence of TiO$_2$, the resulting 6 wt % GO/TiO$_2$ composite supports exhibit no reflections associated with graphene oxide, indicating that the TiO$_2$ nanoparticles successfully inhibit the aggregation of graphene sheets. The A and R notation indicates reflections characteristic of the anatase and rutile polymorphs of TiO$_2$, respectively.

when supported on TiO$_2$ was 5.2 nm with a PSD comparable to values reported previously (see Figure 2).[40] In the absence of any protective surfactant (AuPd/TiO$_2$), the median particle size was slightly lower at 4.7 nm (Supporting Information, Figure S6). For the AuPd−GO/TiO$_2$ series of materials, the mean AuPd particle size progressively decreases from 4.6 to 3.4 nm on increasing the GO content from 1 to 4 wt %. Above 4 wt % GO, the particle size, within experimental error, remained constant. In conjunction with decreasing the mean particle size, the width of the PSDs also narrowed on increasing the GO content. The change in GO concentration must be considered in the context of the composition of the corresponding initial AuPd/GO binary materials. As discussed previously, the 1% AuPd/4% GO/TiO$_2$ catalyst material was formed from a 1:4 AuPd:GO material with the required amount of TiO$_2$ being added to give the ternary catalyst. Consequently, the 1% AuPd/1% GO/TiO$_2$ catalyst would have a significantly higher relative loading of AuPd on GO (1:1 AuPd:GO) before the TiO$_2$ was added, resulting in a far more heavily decorated GO surface and consequently larger metal particles. As the GO concentration increases in the ternary catalysts, the related binary AuPd/GO system has lower metal content. Hence the observed particle size effects are ascribed to the fact that there are a greater number of possible nucleation sites with increasing GO content which generates a greater number of particles with a smaller mean size. In addition, at lower GO contents, the higher fraction, and possibly even saturation, of stabilization sites on the GO surface by AuPd particles would increase the possibility of direct metal NP−TiO$_2$ interactions.

Raman spectroscopy was performed to investigate the effect of the catalyst preparation procedure on the structure of the GO (see Figure 7). Both the GTO precursor and the AuPd−GO/TiO$_2$ catalysts exhibit prominent G (~1595 cm^{-1}) and D (~1360 cm^{-1}) bands, which are caused by the active E$_{2g}$ phonon (in-plane optical mode) of sp^2 carbon and the symmetric A$_{1g}$ mode, respectively. The relative signal strength of these bands depends strongly on the amount of disorder in graphitic materials. Both GTO and AuPd−GO/TiO$_2$ have similar values for the peak frequency and full-width-half-maximum (fwhm) of the D band, as well as the D to G band

maximum intensity ratio (Table S5), indicating that the structure of GO sheets was essentially retained during the preparation of AuPd−GO/TiO$_2$ catalysts.[30] This markedly differs from several metal/GO catalyst preparations, where the GO is significantly reduced and the subsequent defects are reported to provide sites for metal particle nucleation and growth.[26]

Catalysis Using Supported Au−Pd NPs. It has previously been demonstrated that supported AuPd alloy NPs are highly active catalysts for redox reactions.[3,11,41,42] We initially investigated ambient CO oxidation with monometallic Au catalysts (Figure 8), as this reaction is known to be highly sensitive to both NP size and also to the identity of the support used.[43] The activity for the sol-immobilized Au−PVA/TiO$_2$ catalysts was found to be stable at ca. 9.5×10^{-2} min^{-1} (mol$_{CO\ converted}$ mol$_{Au}^{-1}$ min^{-1}) which is a relatively low activity value for an Au/TiO$_2$ catalyst. This poor activity is thought to be due to PVA ligands inhibiting AuPd active sites, and it is now known that the removal of PVA results in a significant improvement in CO conversion.[37] The inhibiting effect of PVA is further inferred by the doubling of activity measured for an Au/TiO$_2$ catalyst prepared by the sol-immobilization technique, but without the addition of PVA or GO. Addition of GO to the Au/TiO$_2$ system can be seen to have a progressively detrimental effect on activity, with the addition of 1% GO having slightly higher activity than the Au−PVA/TiO$_2$ catalyst and 6% GO rendering the catalyst almost inactive. The effect of absolute GO content on catalyst activity, although in itself detrimental for the oxidation of CO, clearly shows that there is a metal−GO interaction occurring that is more apparent with the higher GO loadings. The detrimental effect of GO on the activity toward CO oxidation is not surprising as it is well-known that carbon supports are not best suited to this reaction,[44] while TiO$_2$ is considered to be more viable. So while CO oxidation has provided an insight into the strong metal−GO interactions in this system, other more suitable reactions for carbon supported catalysts have been investigated.

The solvent-free selective oxidation of benzyl alcohol to benzaldehyde has been frequently used as a model oxidation reaction and provides an ideal probe for the behavior of AuPd−GO/TiO$_2$ catalysts. The benzyl alcohol conversion, selectivity to benzaldehyde, turnover number (TON), and benzaldehyde productivity after a 2 h reaction time for the series of AuPd−GO/TiO$_2$ catalysts and reference catalysts are provided in Table 1.

As a point of reference, the conventional AuPd−PVA/TiO$_2$ sol-immobilized catalyst exhibited 72.5% benzyl alcohol conversion and a benzaldehyde productivity of 233 mol kg$_{cat}^{-1}$ h^{-1} at 2 h reaction time, which is consistent with previous reports for this type of material.[45] The AuPd−1% GO/TiO$_2$ catalyst was found to give a relatively low conversion with a benzaldehyde productivity of 162 mol kg$_{cat}^{-1}$ h^{-1}. Increasing the GO content up to 4 wt % resulted in a significant enhancement in conversion while maintaining the selectivity toward benzaldehyde. Increasing the GO content beyond 4% did not lead to any further improvement. It should be noted that AuPd−GO/TiO$_2$ catalysts with >2 wt % GO content all gave higher benzyl alcohol conversions at 2 h than the standard AuPd−PVA/TiO$_2$ material. It is also noteworthy that comparable variations in the PVA stabilizer content (0.65−4.0 wt %) for the conventional sol-immobilized catalyst were found to have no substantial effect on catalytic performance (Supporting Information, Figure S7). Using a fixed GO content
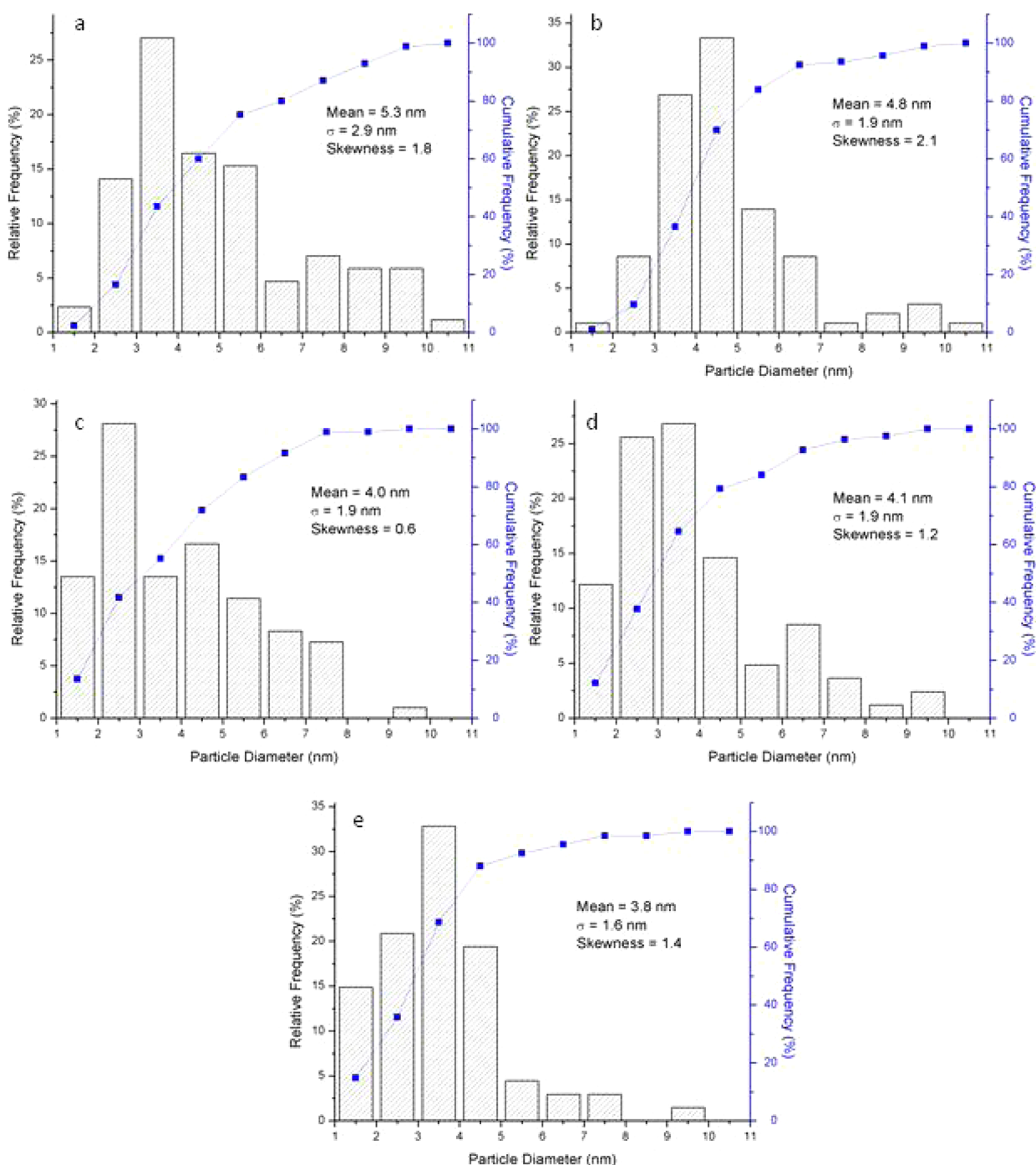
Figure 6. AuPd PSDs for AuPd−GO/TiO$_2$ catalysts having (a) 1%, (b) 2%, (c) 4%, (d) 6%, and (e) 9% GO respectively (100 particles counted).

of 6 wt %, monometallic Au-GO/TiO$_2$ and Pd-GO/TiO$_2$ catalysts were also tested for benzyl alcohol oxidation. The conversion level for both Au−GO/TiO$_2$ and Pd−GO/TiO$_2$ was substantially lower than that for the bimetallic AuPd−GO/TiO$_2$ system (Supporting Information, Figure S8) confirming the strong synergistic effect that has already been seen with Au−Pd alloy catalysts prepared using other more conventional synthesis routes.[10]

The selectivity toward benzaldehyde was found to be essentially the same (ca. 70%) for both the AuPd−PVA/TiO$_2$ and AuPd−GO/TiO$_2$ catalysts. The observed selectivity toward toluene can be attributed to a benzyl alcohol disproportionation pathway in addition to oxidative dehydrogenation of benzyl

alcohol.[45] The facilitation of the disproportionation mechanism with the AuPd−GO/TiO$_2$ series of catalysts was inferred from the observation of equimolar toluene and benzaldehyde production under anaerobic conditions (Supporting Information, Table S6).

GO alone has been previously demonstrated to be active for benzyl alcohol oxidation with a observed TON of 0.016,[20] which is four orders lower than that measured for our AuPd−4 wt % GO/TiO$_2$ catalysts, at ca. 82 (Table 1). Under the same conditions used to test the AuPd−GO/TiO$_2$ catalysts, the 1−9 wt % GO/TiO$_2$ materials gave <0.3% conversion (Supporting Information, Table S7), demonstrating that the primary active component in the composite AuPd−GO/TiO$_2$ catalysts was

Table 1. Particle Size Data and Benzyl Alcohol Oxidation Activity for the Various Supported AuPd Catalysts[a]

catalyst	median (nm)	mean (nm)	conversion (%)	TON[c]	product selectivity (%)		benzaldehyde productivity[d]
					benzaldehyde	toluene	
AuPd−PVA/TiO$_2$	5.2	5.4	72.5	67	69.6	30.1	233
AuPd−PVA/GO			69.5	64	60.7	38.2	195
AuPd/TiO$_2$	4.7	5.0	55.7	52	76.4	23.1	196
AuPd−1% GO/TiO$_2$	4.6	5.3	51.1	47	68.8	30.1	162
AuPd−2% GO/TiO$_2$	4.1	4.8	81.9	76	69.9	29.8	264
AuPd−4% GO/TiO$_2$	3.4	4.0	88.7	82	70.8	28.9	290
AuPd−6% GO/TiO$_2$	3.3	4.1	88.9	82	69.0	30.6	283
used AuPd−6% GO/TiO$_2$[b]	3.4	4.2	86.4	81	70.6	28.2	282
AuPd−9% GO/TiO$_2$	3.6	3.8	87.3	81	70.4	27.0	284
AuPd/GO			57.3	53	60.1	39.3	159
AuPd/GO + TiO$_2$[d]			56.9	53	60.9	38.4	160
AuPd/TiO$_2$ + AuPd/GO[e]			56.9	53	67.6	31.9	161

[a]Reaction conditions: benzyl alcohol to metal molar ratio = 14 000; O$_2$ pressure = 1 bar; 120 °C; 1000 rpm; 2 h. [b]After four usage cycles. [c]Moles of benzyl alcohol reacted per gram AuPd. [d]Moles of benzaldehyde formed per kilogram catalyst hour. [e]AuPd/GO:TiO$_2$ = 1:1 (mass ratio). [f]AuPd/TiO$_2$:AuPd/GO = 1:1 (mass ratio).
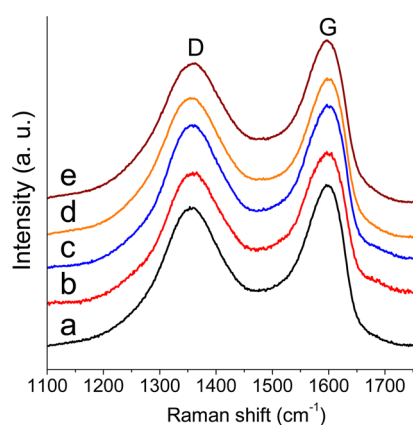

Figure 7. Raman spectra of (a) graphitic oxide (GTO) and a selection of AuPd−GO/TiO$_2$ materials having GO contents of (b) 1%, (c) 2%, (d) 4%, and (e) 6%.

the Au−Pd NPs. Interestingly, when GO was used as a support without the addition of TiO$_2$, the activity of the catalyst was substantially less than that of AuPd−GO/TiO$_2$ catalysts with >2 wt % GO. Although AuPd−GO would have good accessibility of reactants to actives sites, due to the 2-dimensional nature of the NP−GO stabilizer, the lower activity can be explained by the agglomeration of GO sheets into large flakes, due to π−π stacking, thus lowering the accessibility of active sites.[46] As discussed previously the intercalation of TiO$_2$ particles inhibited stacking and agglomeration of the AuPd−GO sheets allowing for faster diffusion of oxygen and alcohols.

Time-online data (Figure 9) for the reference sol-immobilized AuPd−PVA/TiO$_2$ material, the AuPd−GO catalyst, and AuPd−6% GO/TiO$_2$ catalyst clearly illustrates the improved activity when GO and TiO$_2$ are combined in the catalyst formulation. While magnetic iron oxide has been previously added to graphene catalysts to enhance recoverability, an observed improvement in catalytic activity was not noted.[29] The current study directly shows that the addition of
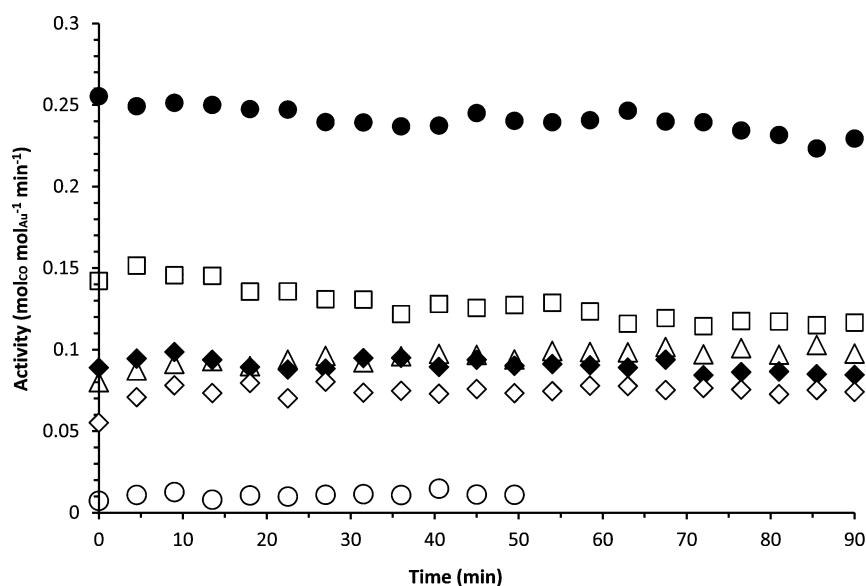

Figure 8. Ambient carbon monoxide (CO) oxidation using Au/TiO$_2$ (●), Au−PVA/TiO$_2$ (◆), and Au/GO/TiO$_2$ catalysts: 1 wt % GO (□), 2 wt % GO (△), 4 wt % GO (◇), and 6 wt % GO (○).
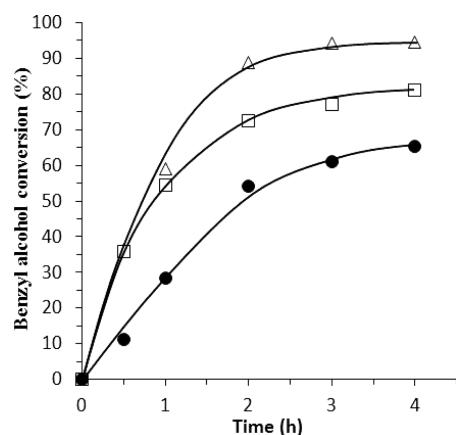
Figure 9. Conversion of benzyl alcohol for AuPd/GO (●); AuPd–PVA/TiO$_2$ (●); AuPd–6% GO/TiO$_2$ (△). Reaction conditions: benzyl alcohol to metal molar ratio = 14 000; O$_2$ pressure = 1 bar; 120 °C; 1000 rpm; 2 h.

the TiO$_2$ metal oxide component significantly improves the activity. However, the improvement in conversion between AuPd–6% GO/TiO$_2$ and AuPd–PVA/TiO$_2$ at 2 h is not observed in the initial rate of the reactions, with both catalysts having the same activity at 0.5 h (TOF of 10 300 h^{-1} for AuPd–PVA/TiO$_2$ and 10 400 h^{-1} for AuPd–6% GO/TiO$_2$). Therefore, while these two catalysts have the same initial activity, the AuPd–6 wt % GO/TiO$_2$ is far more stable under reaction conditions compared to AuPd–PVA/TiO$_2$.

Stability is a very important attribute for any heterogeneous catalyst to have for practical applications. Previous studies on AuPd–PVA/TiO$_2$ catalyst reuse have shown a mild deactivation on repeated usage, although this was considered to be within the error of the analysis.[47] Direct comparison of the deactivation of AuPd–6 wt % GO/TiO$_2$ and AuPd–PVA/TiO$_2$ over four batch catalytic cycles, without a regeneration step (i.e., without washing of catalyst or heat treatment between runs), is shown in Figure 10. The AuPd–6 wt % GO/TiO$_2$ catalyst was shown to be catalytically stable with minimal loss in activity over the four usage cycles, indicating that the catalyst
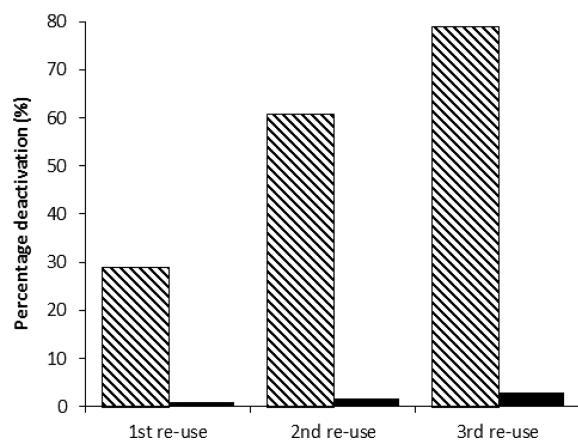

Figure 10. Deactivation, expressed as a percentage of initial activity, of AuPd–6 wt % GO/TiO$_2$ (solid black) and AuPd–PVA/TiO$_2$ (dashed) catalysts over three benzyl alcohol oxidation reuse tests. Each reaction was run under our standard conditions of benzyl alcohol to metal molar ratio = 14 000; O$_2$ pressure = 1 bar; 120 °C; 1000 rpm; 2 h. Initial 2 h conversions are given in Table 1.

was highly stable under reaction conditions. However, the AuPd–PVA/TiO$_2$ catalyst suffered significant deactivation over the four reaction cycles. BF-TEM analysis indicated that the particle size of Au–Pd NPs for both the recovered AuPd–6 wt % GO/TiO$_2$ and AuPd–PVA/TiO$_2$ catalysts was unchanged after four reaction cycles (Table 1 and Supporting Information, Figures S9 and S10).

If the AuPd NP size growth is not the cause of the marked deactivation noted for AuPd–PVA/TiO$_2$ then two other mechanisms are plausible. The first is metal leaching from the support, which has previously been shown *not* to occur for sol-immobilized catalysts in the benzyl alcohol oxidation reaction.[47] Lack of metal leaching was also demonstrated for the AuPd–6 wt % GO/TiO$_2$ catalyst by stopping a reaction at 1 h, removing the catalyst by centrifugation and continuing the reaction with the supernatant, with no further reaction being observed in the absence of catalyst (Figure 11).
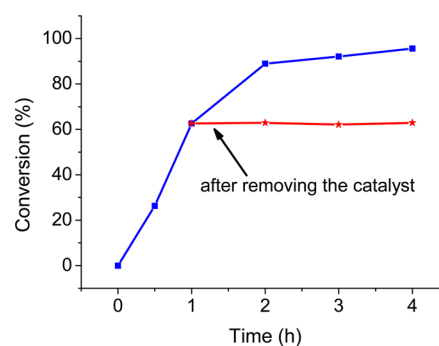

Figure 11. Test to determine homogeneous catalysis contribution in benzyl alcohol oxidation for AuPd–6% GO/TiO$_2$. The line connecting blue squares shows the dependence of benzyl alcohol conversion on the reaction time in the presence of AuPd–6% GO/TiO$_2$. The line connecting red stars indicates the dependence of the benzyl alcohol conversion on reaction time after the catalyst was removed at 1 h.

The second potential cause for deactivation is product inhibition, i.e. the blocking of active sites by products of the benzyl alcohol oxidation reaction. Previously we have shown from diffuse reflectance infrared Fourier transform spectroscopy (DRIFTS) studies that benzoate and benzoic acid species are strongly bound to AuPd–PVA/TiO$_2$ catalysts, even after heating to 280 °C.[48] It is considered that these compounds could block active sites, so a product inhibition study was carried out where 5 mol % of benzoic acid were added at the beginning of the reaction. Interestingly, it was found that the initial turnover frequency (TOF), taken at 0.5 h reaction time, for the standard AuPd–PVA/TiO$_2$ catalyst decreased from 10 300 to 9540 h^{-1} on the addition of benzoic acid. No such decrease in initial turnover frequency was observed for the AuPd–6 wt % GO/TiO$_2$ catalyst, when the reaction mixture was doped with benzoic acid. The adsorption of benzoate species blocking sites on the AuPd–PVA/TiO$_2$ catalyst may not have been observed in previous reuse studies, as a washing step with acetone could have removed these species.[47] The current reuse study did not include a regenerative washing step, resulting in a steady buildup of species capable of blocking active sites.

The decreased level of deactivation observed with the inclusion of GO in the catalyst formulation was further investigated by a temperature-programmed desorption study with DRIFTS (Figure 12 and full band assignment in Table 2),
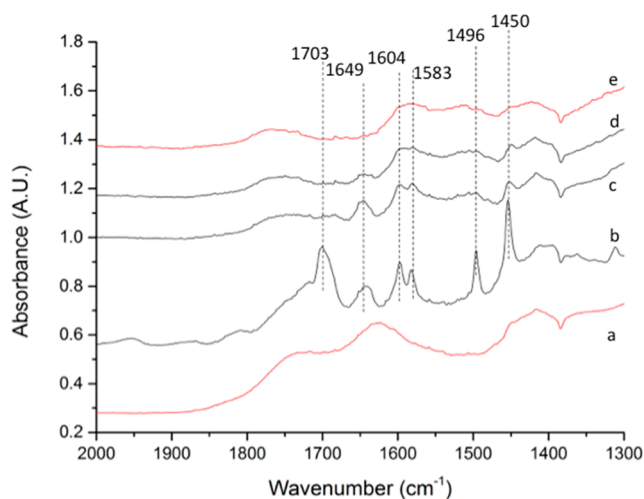
Figure 12. Representative DRIFTS scans of the AuPd−6% GO/TiO₂ catalyst dosed with benzyl alcohol and heat treated under N₂ to 280 °C. (a) Fresh catalyst, (b) dosed catalyst at 100 °C, (c) dosed catalyst at 180 °C, (d) dosed catalyst at 200 °C, and (e) dosed catalyst after 280 °C heat treatment. The vibrational bands associated with AuPd−6% GO/TiO₂ are not labeled.

as previously reported for the AuPd−PVA/TiO₂ catalyst.[48] Heating the catalyst dosed with benzyl alcohol resulted in the loss of bands associated with benzyl alcohol and benzaldehyde by 180 °C. Bands previously assigned to benzoic acid (ν(C═O) at 1654 cm^{-1} and δ(C−H) + ν(C═C) bands at 1452 cm^{-1}) were observed but became progressively less intense on heating and were no longer observable above 200 °C. In comparison, associated bands were still observed after 280 °C heat treatment in the parallel study of the AuPd−PVA/TiO₂ catalyst. This suggests that the possible reaction inhibiting products are less strongly bound on the AuPd−GO/TiO₂ catalyst, explaining the greater resistance of these GO containing materials to deactivation.

Raman spectroscopy analysis of the recovered AuPd−6 wt % GO/TiO₂ catalyst showed a significant change in the integrated area under the D band after a single catalyst run, with the I_D/I_G ratio going from 0.87 to 1.26, in addition to a red shift of ∼44 cm^{-1} and a change in the fwhm of the D band (Figure 13). No further change in GO structure was observed after subsequent reuse tests. This measured variation in relative D band intensity and position correlates with the chemical reduction of GO and is indicative of a decrease in the average size of the sp² domains.[16] As no observable change in catalytic activity was measured between successive reuse tests, it is likely that *either* the activity is not sensitive to the GO structure *or* that reduction occurs very rapidly during initial testing and that the participating form of GO is in fact the reduced state. Changes

in the I_D/I_G ratio and fwhm of the D-band, when correlated with the time-online data for the benzyl alcohol oxidation reaction (Figure 13), show that the reduction of GO starts immediately and is almost complete after 15 min. Further Raman spectroscopy investigation (Supporting Information, Figures S11−14) indicated that the GO component was being reduced by benzyl alcohol as has been previously reported under comparable reaction conditions.[49] It is worth noting that the I_D/I_G ratio (1.27) for the AuPd−6 wt % GO/TiO₂ catalysts after 30 min reaction time was significantly greater than the 0.91 I_D/I_G ratio observed for pure GTO after 30 min reaction time, implying that the Au−Pd NPs present on the GO sheets may also accelerate the reduction of GO (Supporting Information, Figure S14).

Oxidation of a range of alcohol substrates was also performed to investigate the general applicability of AuPd NPs on composite GO/TiO₂ catalyst supports (Table 3). The AuPd−6% GO/TiO₂ catalyst displays superior or comparable initial turnoverfrequencies (TOFs, mol$_{benzyl\ alcohol\ converted}$ mol$_{AuPd}^{-1}$ h^{-1}, calculated at 0.5 h) compared to the sol-immobilized AuPd−PVA/TiO₂ catalyst, demonstrating the general applicability of these new AuPd−GO/TiO₂ catalysts in selective alcohol oxidation.

■ CONCLUSIONS

We have shown that Au−Pd alloy NPs can be stabilized on GO and GO/TiO₂ supports and used as catalysts for the selective oxidation of alcohols. TEM observations confirmed that the supported Au−Pd NPs have narrow particle size distributions, that can be fine-tuned by varying the mass ratio of GO-to-AuPd used during the preparation of AuPd−GO suspension. The GO acts as a two-dimensional stabilizer for the AuPd NPs, unlike the total three-dimensional encapsulation observed with the PVA stabilizer. The addition of TiO₂ significantly improves the activity for the oxidation of benzyl alcohol compared to a pure AuPd−GO composite, as the TiO₂ inhibits regular stacking and excessive agglomeration of the AuPd−GO sheets, to allow for fast diffusion of oxygen and reactants. The ternary AuPd−GO/TiO₂ catalyst was optimized and was demonstrated to have comparable initial activity relative to PVA stabilized Au−Pd NPs supported on TiO₂. Importantly, the AuPd−GO/TiO₂ catalyst is highly stable, with greater time-online stability than the analogous PVA stabilized catalyst, and can be reused for three cycles without any observed loss of activity. The high catalytic activity observed for AuPd−GO/TiO₂ materials may be related to the favorable metal−graphene interaction and the absence of PVA protective ligands on the Au−Pd NP surface permitting improved access to more exposed active metal sites. These studies suggest the very important role of the relatively disordered GO/TiO₂ hybrid nanostructure in enhancing the catalytic activity and stability of the AuPd catalyst. The novel

Table 2. Vibrational Mode Assignment (between 1800 and 1300 cm^{-1}) for the AuPd−6% GO/TiO₂ Sample That Had Been Dosed with Benzyl Alcohol

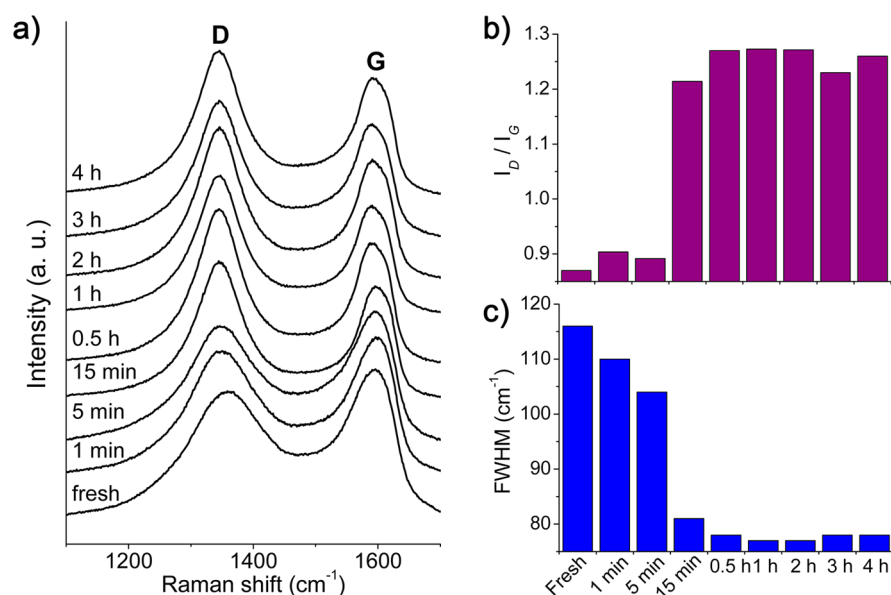| benzyl alcohol	benzaldehyde[a]	toluene[a]	benzoic acid[a]	AuPd−PVA/TiO₂ N₂ flow[a]	AuPd−6 wt % GO/TiO₂ N₂ flow	assignment
	1700		1685	1702, 1654	1703, 1649	ν(C═O)
1607, 1586	1599, 1584	1604	1603, 1584	1598, 1584	1604, 1583	ν(C═C) + δ(C−H)
1496, 1454	1454, 1424	1495, 1458, 1379	1497, 1454, 1424	1496, 1454, 1391	1496, 1450	δ(C−H) + ν(C═C)
1369				1369		δ(O−H)

[a]Data from the literature.[48]

Figure 13. Raman spectroscopy characterization of the AuPd−6 wt % GO/TiO$_2$ catalyst after benzyl alcohol oxidation for various reaction times: (a) Raman spectra; (b) I_D/I_G intensity ratios; and (c) fwhm of the D band.

Table 3. Alcohol Oxidation Activity for the Various Supported AuPd Catalysts Using Different Substrate Molecules[a]

Substrate	Catalyst	TOF (h^{-1})*
Benzyl alcohol	AuPd-PVA/TiO$_2$	10300
	AuPd-6%GO/TiO$_2$	10400
4-Methoxybenzyl alcohol	AuPd-PVA/TiO$_2$	12800
	AuPd-6%GO/TiO$_2$	15000
4-Fluorobenzyl alcohol[b]	AuPd-PVA/TiO$_2$	825
	AuPd-6%GO/TiO$_2$	1100
Cinnamyl alcohol	AuPd-PVA/TiO$_2$	3360
	AuPd-6%GO/TiO$_2$	4070
1-Phenylethanol	AuPd-PVA/TiO$_2$	6000
	AuPd-6%GO/TiO$_2$	6390
Cyclohexanol	AuPd-PVA/TiO$_2$	4130
	AuPd-6%GO/TiO$_2$	4700
1-Octanol[c]	AuPd-PVA/TiO$_2$	207
	AuPd-6%GO/TiO$_2$	228

*Calculated at 0.5 h mol$_{benzyl\ alcohol\ converted}$ mol$_{AuPd}^{-1}$ h^{-1}. [a]Reaction conditions: substrate, 1 g; catalyst, 10 mg; 120 °C; 0.5 h; O$_2$ pressure, 1 bar (relative); 1000 rpm, unless stated specifically. [b]160 °C; 2 h. [c]150 °C; 2 h.

design of this particular composite catalyst support can in principle also be adapted to synthesize a wide range of highly active and stable heterogeneous catalysts for other reactions.

METHODS

Catalyst Preparation. *Starting Materials.* For the preparation of supported Au−Pd alloy catalysts, an aqueous solution containing PdCl$_2$ and HAuCl$_4$ with the desired concentration (typically 0.06 M) was prepared. Fresh solutions of poly vinyl alcohol (PVA) (1 wt % aqueous solution, Aldrich, MW = 10 000, 80% hydrolyzed) and NaBH$_4$ (0.1 M) were also prepared. Graphitic oxide (GTO) was dispersed in water (0.9 mg/mL) and sonicated to form thin GO sheets in solution.[39] The amount of NaBH$_4$ solution added was calculated to give a NaBH$_4$:total metal loading molar ratio of 5:1 in order fully to

reduce the Au and Pd precursors. The molar ratio of Au to Pd was 1:1 in all Au−Pd catalysts and the total metal loading was fixed at 1 wt %.

Immobilization of PVA-Stabilized Au−Pd Nanoparticles on TiO$_2$ (AuPd−PVA/TiO$_2$). The PVA stabilized AuPd nanoparticles were supported on TiO$_2$ (Degussa P25) using a sol-immobilization method.[40] The required amount of PVA solution was added to aqueous solutions of PdCl$_2$ and HAuCl$_4$ of the desired concentration. A freshly prepared solution of NaBH$_4$ was then added to form a dark-brown sol under vigorous stirring. After 30 min of sol generation, the colloid was immobilized by adding TiO$_2$ (acidified to pH 1 with 0.1 M of sulfuric acid). After 1 h, the slurry was filtered and the catalyst was washed thoroughly with a large quantity of distilled water and dried at 120 °C overnight.

Preparation of GO-Stabilized Au−Pd Nanoparticles on TiO₂ (AuPd−GO/TiO₂). A freshly prepared $NaBH_4$ solution was added, with vigorous stirring, to a premixed aqueous solution of $PdCl_2$, $HAuCl_4$, and GO having the desired relative concentrations. A systematic set of samples were prepared with different amounts of GO to give final catalysts containing 1, 2, 4, 6, and 9 wt % of GO. After stirring for 30 min, TiO_2 was added to the GO stabilized Au−Pd NP suspension. After another 1 h of stirring, the catalyst was filtered, washed with a large quantity of distilled water, and dried at 120 °C overnight. Monometallic Au- and Pd-catalysts were also prepared using a similar methodology on the same composite GO/TiO_2 supports.

Preparation of Au−Pd Nanoparticles on GO (1% AuPd/ GO). A freshly prepared $NaBH_4$ solution was added, with vigorous stirring, to a premixed aqueous solution of $PdCl_2$, $HAuCl_4$, and GO having the desired relative concentrations. After stirring for 1 h, the catalyst was recovered by centrifugation (13 000 rpm for 5 min), washed with water, centrifuged a further three times, and then dried at 120 °C overnight. The as-dried material resembles free-supported graphene paper because the GO sheets easily restack together due to the π−π stacking interaction that exists between them.

Catalyst Testing. *Carbon Monoxide Oxidation.* The catalysts were tested for CO oxidation using a fixed-bed microreactor. The reaction temperature was maintained at 30 °C by immersing the U-shaped reactor tube in a thermostatically controlled water bath. 5000 vppm of CO in air (containing ca. 1000 ppm of H_2O) and a gas hourly space velocity of 12 000 h^{-1} (50 mg catalyst, flow rate of 21 mL min^{-1}) was used. The reactor temperature was maintained isothermally at 30 °C using a water bath. Analysis of reactants and products was performed using online gas chromatography (Varian CP-3800).

Alcohol Oxidation. Alcohol oxidation was performed under solvent free conditions in a 50 mL glass round-bottom flask on a Radleys carousel. Typically, the alcohol and the catalyst were charged into the reactor which was then purged three times with oxygen. The reactor was sealed and the pressure was maintained at 1 bar (relative pressure). During the reaction, the pressure was monitored via a pressure gauge to ensure that there were no pressure fluctuations. The glass reactor containing the reaction mixture was loaded into a preheated heating block, which was maintained at 120 °C with a stirring speed of 1000 rpm. After a specific reaction period, the reactor was quickly cooled in an ice bath and held there for 10 min. The reactor was then opened and the contents centrifuged. An aliquot of the clear supernatant reaction mixture (0.5 mL) was then diluted with mesitylene (0.5 mL) for GC analysis. It was verified that no reaction occurred in the absence of the Au−Pd NPs or in the presence of the catalyst support alone. This experimental method is identical to the standard reaction protocols for the solvent-free oxidation of benzyl alcohol that have been reported elsewhere.[10,40]

Metal Leaching Tests. It is sometimes possible for active components of a heterogeneous catalyst system to leach into the reaction mixture during the reaction, resulting in the formation of an active homogeneous catalyst or the deactivation/decrease in activity of the heterogeneous catalyst. To confirm that the observed oxidation catalysis of benzyl alcohol is truly caused by the heterogeneous GO stabilized AuPd/TiO₂ catalyst the following experiment was performed. The oxidation of benzyl alcohol was carried out using AuPd−

6% GO/TiO₂ material at 120 °C. After 1 h, the catalyst was removed by centrifugation. The clean supernatant was returned to the reactor and no increase of benzyl alcohol conversion was observed during the subsequent 3 h of reaction, indicating that the solution phase did not include any catalytically active homogeneous species.

Catalyst Reuse Studies. To check if the catalyst was capable of retaining its original activity after the reaction, a series of reuse experiments were carried out. A 10 mg portion of the AuPd−6% GO/TiO₂ material was used for benzyl alcohol oxidation for 2 h. The reaction mixture was centrifuged to separate out the catalyst, and the residual clean supernatant was then analyzed by GC. Next, fresh benzyl alcohol was then added to the flask containing this recovered, unwashed catalyst and a new benzyl alcohol oxidation was performed for 2 h duration. The catalyst was recovered and used again for a third time without any evident loss of catalytic activity.

Catalyst Characterization. *Raman Spectroscopy.* Samples were mounted on an aluminum slide and analyzed using a Renishaw in-via Ramascope with an excitation laser wavelength of 514 nm and a laser intensity of 10%. The sample was scanned using an attenuation time of 5 and 50 sequential scans were carried out to generate a spectrum.

Transmission Electron Microscopy (TEM) Analyses. Samples were prepared for electron microscopy examination by dispersing the catalyst powder in ultrahigh purity ethanol. A drop of the suspension was then allowed to evaporate on a carbon microgrid supported by a 300 mesh copper grid. Samples were examined in a JEOL JEM 2100F transmission electron microscope operating at an accelerating voltage of 200 kV. This instrument was also fitted with an Oxford Instruments energy-dispersive X-ray spectrometer (XEDS) for compositional analysis.

Scanning Electron Microscopy (SEM) Analyses. The morphology of the catalysts was observed by scanning electron microscopy (SEM) using on an FEI field emission Magellan 400 SEM equipped with an Oxford Instruments XEDS system. The sample was dispersed in ultrahigh purity ethanol, and then a drop of the suspension was dropped onto a carbon micro grid supported by a 300 mesh copper grid. SEM images of the recovered catalyst are presented in the Supporting Information.

X-ray Photoelectron Spectroscopy (XPS). XPS measurements were recorded on a VG EscaLab 220i spectrometer, using a standard Al Kα X-ray source (300 W) and analyzer pass energy of 20 eV. Samples were mounted using double-sided adhesive tape and binding energies are referenced to the carbon (1s) binding energy of adventitious carbon taken to be 284.7 eV.

X-ray Diffraction (XRD). Powder X-ray diffraction (XRD) patterns were recorded using a Panalytical X'pert Pro diffractometer using Ni filtered Cu Kα radiation (operating at 40 kV, 40 mA). The XRD patterns of GTO and 6 wt % GO/ TiO₂ are shown in the Supporting Information.

Elemental Analysis. The Au and Pd content in the composites were analyzed using an Agilent 4100 microwave plasma-atomic emission spectrometer.

Diffuse Reflectance Infrared Fourier Transform Spectroscopy. DRIFTS studies were performed using a Bruker Tensor 27 spectrometer fitted with a HgCdTe (MCT) detector and a Harrick Praying Mantis HVC-DRP-4 cell equipped with ZnSe windows. Samples were mixed with benzyl alcohol and added to the cell. After an initial scan at room temperature, the sample was heated to 280 °C at 1 °C min^{-1} under an atmosphere of

flowing N_2 (20 mL min^{-1}) or O_2 (20 mL min^{-1}) with flow rates regulated by Bronkhorst mass flow meters. Spectra were run in the range of 4000−600 cm^{-1}, with 64 accumulation scans, every 10 °C.

■ ASSOCIATED CONTENT

Ⓢ Supporting Information

The Supporting Information is available free of charge on the ACS Publications website at DOI: 10.1021/acscatal.5b00480.

> Structural schemes for GO, AuPd−GO, and AuPd−PVA composite; additional TEM, PSD, and XRD data on the catalysts; additional benzyl alcohol oxidation for various Au−Pd catalysts and reference catalysts; and effects of reaction conditions on the catalyst structures, Raman analyses (PDF)

■ AUTHOR INFORMATION

Corresponding Author

*E-mail: hutch@cardiff.ac.uk.

Notes

The authors declare no competing financial interest.

■ ACKNOWLEDGMENTS

■ REFERENCES

(1) Sinha, A. K.; Seelan, S.; Tsubota, S.; Haruta, M. *Angew. Chem., Int. Ed.* **2004**, *43*, 1546−1548.

(2) Hughes, M. D.; Xu, Y. J.; Jenkins, P.; McMorn, P.; Landon, P.; Enache, D. I.; Carley, A. F.; Attard, G. A.; Hutchings, G. J.; King, F.; Stitt, E. H.; Johnston, P.; Griffin, K.; Kiely, C. J. *Nature* **2005**, *437*, 1132−1135.

(3) Kesavan, L.; Tiruvalam, R.; Ab Rahim, M. H.; bin Saiman, M. I.; Enache, D. I.; Jenkins, R. L.; Dimitratos, N.; Lopez-Sanchez, J. A.; Taylor, S. H.; Knight, D. W.; Kiely, C. J.; Hutchings, G. J. *Science* **2011**, *331*, 195−199.

(4) Rahim, A.; Hasbi, M.; Forde, M. M.; Jenkins, R. L.; Hammond, C.; He, Q.; Dimitratos, N.; Lopez-Sanchez, J. A.; Carley, A. F.; Taylor, S. H. *Angew. Chem.* **2013**, *125*, 1318−1322.

(5) Biella, S.; Prati, L.; Rossi, M. *J. Catal.* **2002**, *206*, 242−247.

(6) Porta, F.; Prati, L. *J. Catal.* **2004**, *224*, 397−403.

(7) Haruta, M.; Yamada, N.; Kobayashi, T.; Iijima, S. *J. Catal.* **1989**, *115*, 301−309.

(8) Landon, P.; Collier, P. J.; Papworth, A. J.; Kiely, C. J.; Hutchings, G. J. *Chem. Commun.* **2002**, 2058−2059.

(9) Edwards, J. K.; Freakley, S. J.; Carley, A. F.; Kiely, C. J.; Hutchings, G. J. *Acc. Chem. Res.* **2014**, *47*, 845−854.

(10) Enache, D. I.; Edwards, J. K.; Landon, P.; Solsona-Espriu, B.; Carley, A. F.; Herzing, A. A.; Watanabe, M.; Kiely, C. J.; Knight, D. W.; Hutchings, G. J. *Science* **2006**, *311*, 362−365.

(11) Edwards, J. K.; Hutchings, G. J. *Angew. Chem., Int. Ed.* **2008**, *47*, 9192−9198.

(12) Novoselov, K. S.; Geim, A. K.; Morozov, S. V.; Jiang, D.; Zhang, Y.; Dubonos, S. V.; Grigorieva, I. V.; Firsov, A. A. *Science* **2004**, *306*, 666−669.

(13) Li, X.; Zhu, Y.; Cai, W.; Borysiak, M.; Han, B.; Chen, D.; Piner, R. D.; Colombo, L.; Ruoff, R. S. *Nano Lett.* **2009**, *9*, 4359−4363.

(14) Lee, C.; Wei, X.; Kysar, J. W.; Hone, J. *Science (Washington, DC, U. S.)* **2008**, *321*, 385−388.

(15) Balandin, A. A.; Ghosh, S.; Bao, W.; Calizo, I.; Teweldebrhan, D.; Miao, F.; Lau, C. N. *Nano Lett.* **2008**, *8*, 902−907.

(16) Stankovich, S.; Dikin, D. A.; Piner, R. D.; Kohlhaas, K. A.; Kleinhammes, A.; Jia, Y.; Wu, Y.; Nguyen, S. B. T.; Ruoff, R. S. *Carbon* **2007**, *45*, 1558−1565.

(17) Shin, H.-J.; Kim, K. K.; Benayad, A.; Yoon, S.-M.; Park, H. K.; Jung, I.-S.; Jin, M. H.; Jeong, H.-K.; Kim, J. M.; Choi, J.-Y.; Lee, Y. H. *Adv. Funct. Mater.* **2009**, *19*, 1987−1992.

(18) Wang, G.; Yang, J.; Park, J.; Gou, X.; Wang, B.; Liu, H.; Yao, J. *J. Phys. Chem. C* **2008**, *112*, 8192−8195.

(19) Loh, K. P.; Bao, Q.; Eda, G.; Chhowalla, M. *Nat. Chem.* **2010**, *2*, 1015−1024.

(20) Dreyer, D. R.; Jia, H.-P.; Bielawski, C. W. *Angew. Chem.* **2010**, *122*, 6965−6968.

(21) Pyun, J. *Angew. Chem., Int. Ed.* **2011**, *50*, 46−48.

(22) Kamat, P. V. *J. Phys. Chem. Lett.* **2010**, *1*, 520−527.

(23) Scheuermann, G. M.; Rumi, L.; Steurer, P.; Bannwarth, W.; Mülhaupt, R. *J. Am. Chem. Soc.* **2009**, *131*, 8262−8270.

(24) Zhang, N.; Qiu, H.; Liu, Y.; Wang, W.; Li, Y.; Wang, X.; Gao, J. *J. Mater. Chem.* **2011**, *21*, 11080−11083.

(25) Siamaki, A. R.; Khder, A. E. R. S.; Abdelsayed, V.; El-Shall, M. S.; Gupton, B. F. *J. Catal.* **2011**, *279*, 1−11.

(26) Moussa, S. O.; Panchakarla, L. S.; Ho, M. Q.; El-Shall, M. S. *ACS Catal.* **2014**, *4*, 535−545.

(27) Li, Y.; Gao, W.; Ci, L.; Wang, C.; Ajayan, P. M. *Carbon* **2010**, *48*, 1124−1130.

(28) Seger, B.; Kamat, P. V. *J. Phys. Chem. C* **2009**, *113*, 7990−7995.

(29) Elazab, H. A.; Siamaki, A. R.; Moussa, S.; Gupton, B. F.; El-Shall, M. S. *Appl. Catal., A* **2015**, *491*, 58−69.

(30) Dreyer, D. R.; Park, S.; Bielawski, C. W.; Ruoff, R. S. *Chem. Soc. Rev.* **2010**, *39*, 228−240.

(31) Cote, L. J.; Kim, J.; Zhang, Z.; Sun, C.; Huang, J. *Soft Matter* **2010**, *6*, 6096−6101.

(32) Porta, F.; Prati, L.; Rossi, M.; Coluccia, S.; Martra, G. *Catal. Today* **2000**, *61*, 165−172.

(33) Lopez-Sanchez, J. A.; Dimitratos, N.; Miedziak, P.; Ntainjua, E.; Edwards, J. K.; Morgan, D.; Carley, A. F.; Tiruvalam, R.; Kiely, C. J.; Hutchings, G. J. *Phys. Chem. Chem. Phys.* **2008**, *10*, 1921−30.

(34) Hutchings, G. J.; Kiely, C. J. *Acc. Chem. Res.* **2013**, *46*, 1759−1772.

(35) Menard, L. D.; Xu, F.; Nuzzo, R. G.; Yang, J. C. *J. Catal.* **2006**, *243*, 64−73.

(36) Grunwaldt, J. D.; Kiener, C.; Wögerbauer, C.; Baiker, A. *J. Catal.* **1999**, *181*, 223−232.

(37) Lopez-Sanchez, J. A.; Dimitratos, N.; Hammond, C.; Brett, G. L.; Kesavan, L.; White, S.; Miedziak, P.; Tiruvalam, R.; Jenkins, R. L.; Carley, A. F.; Knight, D.; Kiely, C. J.; Hutchings, G. J. *Nat. Chem.* **2011**, *3*, 551−556.

(38) Sankar, M.; He, Q.; Morad, M.; Pritchard, J.; Freakley, S. J.; Edwards, J. K.; Taylor, S. H.; Morgan, D. J.; Carley, A. F.; Knight, D. W.; Kiely, C. J.; Hutchings, G. J. *ACS Nano* **2012**, *6*, 6600−6613.

(39) Hummers, W. S.; Offeman, R. E. *J. Am. Chem. Soc.* **1958**, *80*, 1339−1339.

(40) Pritchard, J.; Kesavan, L.; Piccinini, M.; He, Q.; Tiruvalam, R.; Dimitratos, N.; Lopez-Sanchez, J. A.; Carley, A. F.; Edwards, J. K.; Kiely, C. J.; Hutchings, G. J. *Langmuir* **2010**, *26*, 16568−16577.

(41) Dimitratos, N.; Lopez-Sanchez, J. A.; Hutchings, G. J. *Chem. Sci.* **2012**, *3*, 20−44.

(42) Brett, G. L.; He, Q.; Hammond, C.; Miedziak, P. J.; Dimitratos, N.; Sankar, M.; Herzing, A. A.; Conte, M.; Lopez-Sanchez, J. A.; Kiely, C. J.; Knight, D. W.; Taylor, S. H.; Hutchings, G. J. *Angew. Chem., Int. Ed.* **2011**, *50*, 10136−10139.

(43) Louis, C. In *Gold nanoparticles: recent advances in CO oxidation*; Wiley-VCH Verlag GmbH & Co. KGaA: 2008; pp 475−503.

(44) Okumura, M.; Tsubota, S.; Haruta, M. *J. Mol. Catal. A: Chem.* **2003**, *199*, 73−84.

(45) Sankar, M.; Nowicka, E.; Tiruvalam, R.; He, Q.; Taylor, S. H.; Kiely, C. J.; Bethell, D.; Knight, D. W.; Hutchings, G. J. *Chem. - Eur. J.* **2011**, *17*, 6524−6532.

(46) Dikin, D. A.; Stankovich, S.; Zimney, E. J.; Piner, R. D.; Dommett, G. H. B.; Evmenenko, G.; Nguyen, S. B. T.; Ruoff, R. S. *Nature* **2007**, *448*, 457−460.

(47) Dimitratos, N.; Lopez-Sanchez, J. A.; Morgan, D.; Carley, A. F.; Tiruvalam, R.; Kiely, C. J.; Bethell, D.; Hutchings, G. *J. Phys. Chem. Chem. Phys.* **2009**, *11*, 5142−53.

(48) Nowicka, E.; Hofmann, J. P.; Parker, S. F.; Sankar, M.; Lari, G. M.; Kondrat, S. A.; Knight, D. W.; Bethell, D.; Weckhuysen, B. M.; Hutchings, G. *J. Phys. Chem. Chem. Phys.* **2013**, *15*, 12147−55.

(49) Dreyer, D. R.; Murali, S.; Zhu, Y.; Ruoff, R. S.; Bielawski, C. W. *J. Mater. Chem.* **2011**, *21*, 3443−3447.